Available online at www.sciencedirect.com
ScienceDirect
Journal of Nuclear Materials 361 (2007) 141–148
journal of nuclear materials
www.elsevier.com/locate/jnucmat

Helium bubble nucleation in bcc iron studied by kinetic Monte Carlo simulations

Chaitanya S. Deo [a,*], Maria A. Okuniewski [b], Srinivasan G. Srivilliputhur [a], Stuart A. Maloy [a], Michael I. Baskes [a], Michael R. James [a], James F. Stubbins [b]

[a] *Los Alamos National Laboratory, Los Alamos, NM 87545, USA*
[b] *Department of Nuclear, Plasma and Radiological Engineering, University of Illinois at Urbana-Champaign, Urbana, IL 61801, USA*

Abstract

Fast reactors and other advanced nuclear systems are increasingly considering the use of ferritic and ferritic–martensitic steels for cladding and structural applications. For these materials applications, radiation damage and relatively large amounts of helium generated during the irradiation damage process are recognized to be major issues with materials durability and performance. In these cases, irradiation damage alone is significant; however the added effect of helium on the accumulation of defects and defect clusters can dramatically imact the effect of the resulting microstructure on physical and mechanical properties. Using a kinetic Monte Carlo method we study embryonic bubble nucleation under irradiation damage conditions and helium generation. Migration of helium, vacancies, self interstitial atoms and their clusters is included in the kinetic Monte Carlo model. We estimate embryonic bubble density, interstitial cluster density and embryonic bubble size as a function of the helium content and displacements per atom. Bubble density and size increases with increasing helium content; there is a slight increase in interstitial cluster density as well.

PACS: 61.72.Cc; 61.72.Ji; 61.82.bg; 02.70.Uu; 05.10.Ln; 66.30.Jt

1. Introduction

Fast reactors and other advanced nuclear systems are increasingly considering the use of ferritic and ferritic–martensitic steels for cladding and structural applications. For these materials applications, radiation damage and relatively large amounts of helium generated during the irradiation damage process are recognized to be major issues with materials durability and performance. In these cases, irradiation damage alone is significant; however the added effect of impurities on the accumulation of defects and defect clusters can dramatically imact the effect of the resulting microstructure on physical and mechanical properties. The interaction of interstitial impurity atoms with radiation-produced defects in bcc metals and its influence on radiation hardening and embrittlement have been well studied and reviewed by Wechsler and Murty [1] where special emphasis was placed on the role of oxygen in vanadium and niobium and of nitrogen and carbon in

* Corresponding author. Address: Los Alamos National Laboratory, P.O. Box 1663, MS G755, Los Alamos, NM 87545, USA.
E-mail address: cdeo@lanl.gov (C.S. Deo).

0022-3115/$ - see front matter © 2007 Published by Elsevier B.V.
doi:10.1016/j.jnucmat.2006.12.018

iron and steel. Helium is a much lighter atom than these impurities and tends to stabilize vacancy clusters that lead to a decrease in mechanical properties of the cladding and structures [2–6].

Fusion reactor and accelerator driven system materials will experience high generations of helium (10 and 150 appm/dpa, respectively) due to the occurrence of radiation damage processes. Ferritic steels are candidate materials for these systems because of their resistance to void swelling, irradiation creep, and helium and hydrogen embrittlement at higher temperatures ($T/T_m > 0.4$). However, these alloys exhibit a large increase in yield stress and ductile to brittle transition temperature at lower irradiation temperatures ($T_{irr} < 500$ °C). These property changes are not well understood and may be related to helium generation and bubble formation [7,8].

The evolution of materials damage associated with continuous helium implantation and irradiation is characterized by several stages of microstructural evolution. These stages have been enumerated by Trinkaus et al. [9,10] and are bubble incubation, bubble nucleation, bubble growth, cavity growth and crack growth stages. Since the bubble densities in the nucleation period are substantial for the subsequent periods, an understanding of the latter stages requires a detailed knowledge of the incubation and nucleation stages of microstructural evolution.

The present work is aimed at quantifying the effects of irradiation damage accumulation in the presence of helium in ways that were not possible in earlier studies. This is accomplished through systematic and coordinated computational modeling and experiments. The modeling approach employs both molecular dynamics (MD) and kinetic Monte Carlo (kMC) simulations to study the dynamic evolution of helium and defect clusters in bcc iron over relevant time scales. Fig. 1 shows connections between various levels of modeling and simulation as applied to radiation damage in ferritic steels.

In this paper, we will focus on a lattice based kinetic Monte Carlo (kMC) to simulate the long-term diffusion of vacancies, self interstitials and helium in displacement cascades and the modification of defect evolution by the presence of helium in body centered cubic (bcc) iron. Kinetic Monte Carlo models and simulations have been employed to study cascade ageing and defect accumulation at low doses using the input from atomistic simula-

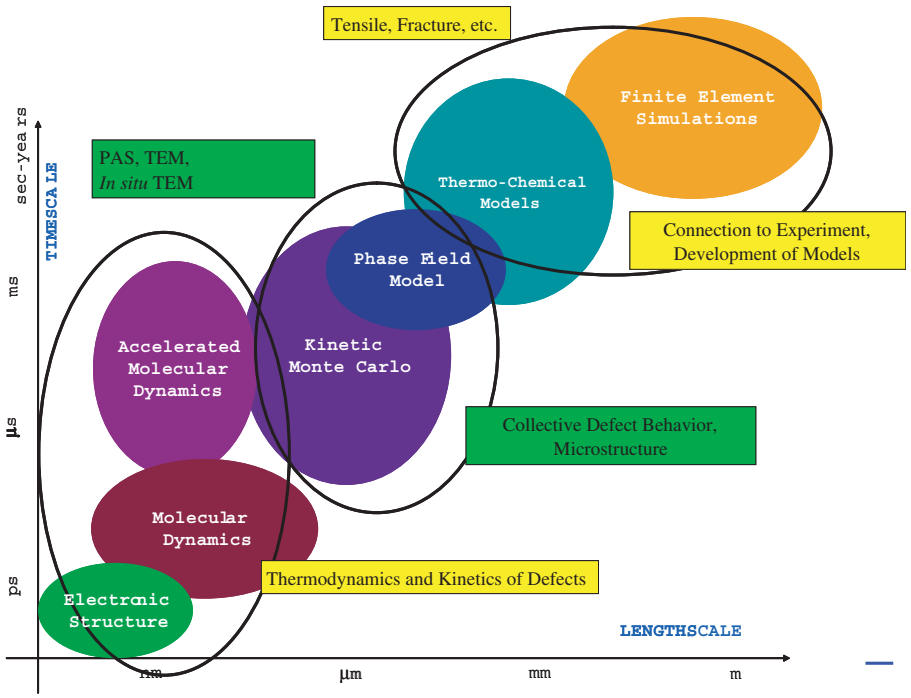

Fig. 1. Various computer modeling techniques that are coupled together to reach experimentally observable time and length scales and the experimental techniques that can be used to validate these models.

tions of cascades and defect migration properties [11–18]. These have mostly focused on intrinsic defect (interstitial and vacancy) migration, clustering and annihilation under irradiation conditions.

For the Fe–He system, modeling of helium clusters has been performed by Morishita et al. [19,20] and Bringa et al. [21] using semi-empirical potentials. In one paper, Morishita et al. [20] performed molecular dynamics (MD) calculations to evaluate the thermal stability of helium–vacancy clusters in Fe. In another paper, Morishita et al. [19] have looked at dissolution of helium–vacancy clusters as a function of temperature increase using the empirical potentials for the Fe–He system. Wirth and Bringa [22] have simulated the motion of one single 2He–3Vac cluster at 1000 K using the same potential system. First principles calculations of helium atoms in interstitial and substitutional sites has been performed by Fu and Willaime [23] and can be used to provide an input parameter set for kinetic Monte Carlo calculations. In this paper, we analyze the effect of helium generation and migration on the microstructural evolution of bcc iron under irradiation conditions especially the formation of embryonic bubbles under continuous damage conditions.

2. Simulation model and algorithm

The kinetic Monte Carlo model consists of helium interstitials on the octahedral sublattice and vacancies on the bcc iron lattice. Fig. 2 shows the mechanisms by which the point defects migrate. The migration of the free (not clustered) helium is shown in Fig. 2(a) and that of the vacancies and self interstitial atoms is shown in Fig. 2(b). The lowest-energy migration path of the SIA corresponds to a nearest-neighbor translation–rotation jump in the ⟨1 1 1⟩ direction. The rates of migration of the point defect entities are calculated as

$$r^{\mathrm{i}}_{\mathrm{migration}} = \nu^{\mathrm{i}}_{\mathrm{migration}} \exp\left(-\frac{E^{\mathrm{i}}_{\mathrm{migration}}}{k_{\mathrm{B}}T}\right), \qquad (1)$$

where the superscript i refers to the helium, self interstitial atoms and the vacancy point defect entities. The rate of migration of the point defect entity is $r^{\mathrm{i}}_{\mathrm{migration}}$, the attempt frequency is $\nu^{\mathrm{i}}_{\mathrm{migration}}$, the migration barrier is $E^{\mathrm{i}}_{\mathrm{migration}}$, while k_{B} and T are the Boltzmann constant and the temperature, respectively. Two point defect entities are considered to be in a cluster when the distance between them is less than

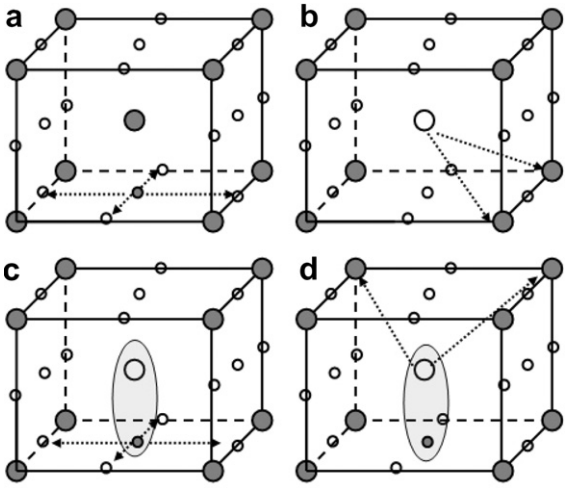

Fig. 2. The basic mechanisms of helium and vacancy activity in single crystal bcc iron. Large filled circles represent iron, large open circles represent vacancies, small filled circles represent helium atoms and small open circles represent the octahedral bcc sites. (a) Helium migration on the octahedral sublattice. (b) Vacancy and self interstitial migration in bcc iron. (c) Dissociation of helium from an embryonic bubble. (d) Dissociation of vacancy from an embryonic bubble.

a_0, which is the lattice constant of bcc iron. Interstitial atoms are not allowed to dissociate from clusters. Dissociation of the helium and the vacancy from the cluster is described in Fig. 2(c) and (d), respectively. The rate of dissociation of a point defect entity (i = helium or vacancy) from a cluster into the bulk lattice is considered to be thermally activated and is calculated as:

$$r^{\mathrm{i}}_{\mathrm{dissociation}} = \nu^{\mathrm{i}}_{\mathrm{dissociation}} \exp\left(-\frac{E^{\mathrm{i}}_{\mathrm{dissociation}}}{k_{\mathrm{B}}T}\right), \qquad (2)$$

where $r^{\mathrm{i}}_{\mathrm{dissociation}}$ is the rate or dissociation, $\nu^{\mathrm{i}}_{\mathrm{dissociation}}$ is the attempt frequencies, $E^{\mathrm{i}}_{\mathrm{dissociation}}$ is the energy of dissociation. The dissociation energy $E^{\mathrm{i}}_{\mathrm{dissociation}}$ of a point defect from a cluster is taken to be the sum of the energy to bind a point defect entity to the cluster and $E^{\mathrm{i}}_{\mathrm{migration}}$. Small bubbles migrate with a Arrhenius migration rate parameterized by Table 1. Larger bubbles migrate by surface diffusion at the bubble–matrix interface [24,25],

$$D_{\mathrm{B}} = D_{\mathrm{S}}\left(\frac{3\Omega^{4/3}}{2\pi r^4}\right), \qquad (3)$$

where D_{B} and D_{s} are the bubble and surface diffusivities, respectively, Ω is the atomic volume and r the radius of the bubble.

Table 1
A table of the events included in the kinetic Monte Carlo model

Entity	Event	E (eV)	v_0 (s^{-1})	Remarks
Helium	Migration	0.078	1e14	Helium migrates on the interstitial sublattice
Vacancy	Migration	0.65	6e13	Vacancy migration on the substitutional sublattice
SIA	Migration	0.3	6e13	SIA migration on the substitutional sublattice
Helium	Dissociation from He_nV_m	2.0	1e14	Helium dissociation from the He–V cluster
Vacancy	Dissociation from He_nV_m	2.0	6e13	Vacancy dissociation from the helium–vacancy cluster
Helium	Dissociation from He_n	0.30	1e14	Helium dissociation from the helium–helium cluster
Vacancy	Dissociation from V_m	0.20	6e13	Vacancy dissociation from the vacancy cluster
Interstitial clusters	1D migration	0.1	6e13	Interstitial clusters up to size four are considered mobile
He–V clusters	3D migration	1.1	1e14	Clusters containing up to three vacancies atoms migrate according to this rate
He–V clusters	3D migration	–	–	Diffusivity of clusters containing more than three vacancies calculated by considering surface diffusion mechanisms (Eq. (3))

Migration energies and attempt frequencies are provided where applicable.

Morishita et al. [20] and Fu and Willaime [23] have calculated the migration energies of helium and vacancies as well as the binding energies of some helium–vacancy clusters. We employ these migration barriers to calculate the rate of migration of the point defect entities. Parameters used to calculate these quantities are described in Table 1. These parameters are used to calculate the rates migration and dissociation events (Eqs. (1)–(3)) in the system and build the event catalog for the kMC simulation.

The event catalog is generated by calculating the rates of migration or dissociation of the point defect entities using Eqs. (1)–(3). The kMC event catalog consists of the migration, clustering and dissociation of the point defect entities, helium, self interstitial atoms and vacancies. The transition probability of each event is proportional to the rate of event occurrence, calculated by the Eqs. (1)–(3). We follow the well established kMC simulation algorithm [26,27] which is a stochastic, atomic-scale method to simulate the time-evolution of defects and nano/microstructural evolution that focuses on individual defects and not on atomic vibrations.

Reaction pathways available in the system are tabulated in Table 1. Rates of migration of events are calculated at each kMC step. Parameters are obtained both from literature using first principles calculations [23,28] and also from molecular statics calculations using semi-empirical potentials as employed by Morishita et al. [19] and Wirth and Bringa [22] (using the Ackland Finnis–Sinclair potential, the Wilson–Johnson potential and the Ziegler–Biersack–Littmark–Beck potential for describing the interactions of Fe–Fe, Fe–He and He–He, respectively). Helium atoms are introduced at random positions at the beginning of the simulation. Self interstitial atoms (SIA) are produced in the simulation along with vacancies as Frenkel pairs as cascade debris. Self interstitial atoms are mobile and cluster. Self interstitial clusters up to size five migrate one dimensionally. Self interstitials of higher size are stationary. Mono- and clustered vacancies are mobile. Vacancies can dissociate from a vacancy cluster as well as a helium–vacancy cluster. Helium atoms migrate on the octahedral sublattice as well as part of helium–vacancy bubbles. A substitutional helium is considered as a 1–1 He_1V_1 and is mobile. If a bubble has a helium–vacancy ratio greater than five, it emits a self interstitial atom. Small bubbles migrate according to Eq. (1) and Table 1 while large bubbles migrate according to Eq. (3). Self interstitial atoms and vacancies annihilate when they meet either as point defects or in a cluster. The boundary of the simulation cell acts as a sink for the point defect entities.

At each kMC step, the system is monitored to identify a clustering event. When two point defect entities (helium–helium, vacancy–vacancy, helium–vacancy) are in a cluster the simulation creates a mapping between the entities and the cluster such that for each cluster there are at least two entities

associated with the cluster. The event catalog is updated with the new rates of event occurrence and the transition probabilities for the next kMC event are calculated using Eqs. (1)–(3) using the parameters from Table 1.

Simulations were performed for a damage energy of 100 keV. A production rate of randomly distributed cascades is assumed such that the damage is introduced at a rate of 10^{-6} dpa/s. The simulation cell size is $400a_0 \times 400a_0 \times 400a_0$, where a_0 is the lattice parameter of iron. The number of Frenkel pairs introduced in the simulation cell are calculated by the Norgett–Robinson–Torrens relationship,

$$\text{Displacements per cascade} = \frac{0.8E_D}{2E_d}, \tag{4}$$

where E_D is the energy of incident particles while E_d is the threshold energy (40 eV for iron [29]). Initial concentration of helium is a parameter in the simulation and is varied from 1 to 25 appm/dpa. Damage that accumulates in the system is another parameter in the system and determines the length of the simulation. The incident energy is also a simulation control parameter that determines the number of defects introduced in a single cascade. The simulation is performed until sufficient damage is accumulated in the simulation cell.

3. Results

We now employ the kMC model to simulate the effect of damage and helium/dpa ratios on the formation of bubbles and bubble density. Simulations are performed for values of the He concentrations varying from 1 to 25 appm/dpa (appm = atomic parts per million). Initial concentrations of both point defect entities are calculated from the NRT formula (Eq. (4)) using an incident energy of 100 keV. Overall damage is introduced at the rate of 10^{-6} dpa/s and the simulation is carried out until the required amount of damage has accumulated in the system.

Fig. 3 shows the concentration of bubbles as a function of He concentration (appm/dpa) after damage equal to 0.1 and 1 dpa is introduced. The simulation temperature is 0.3 T_m. The bubble density increases with increasing He/dpa ratio. The bubble density can be described by a power law expression,

$$c_B = K(c_{He})^m, \tag{5}$$

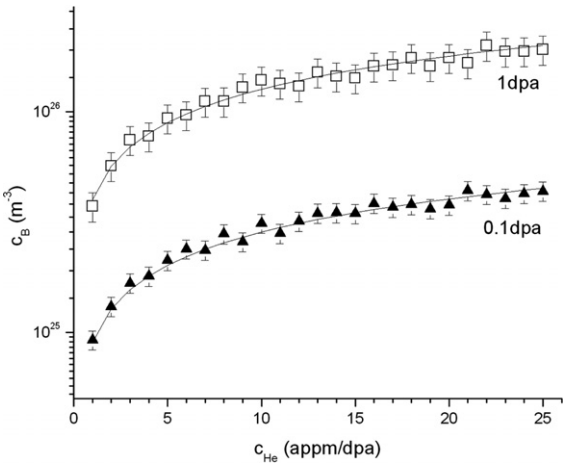

Fig. 3. A plot of the concentration of bubbles (c_B) as a function of helium concentration (expressed in terms of appm/dpa) for two damage levels, 0.1 dpa (filled triangles) and 1 dpa (open squares). The line is a fit to the data assuming a square root dependence of the bubble density on helium concentration. The simulation temperature is 543 K (0.3 T_m, the melting temperature for iron).

where c_B is the bubble density, c_{He} is the helium concentration expressed as appm He/dpa and K and m are constants determined by the kinetic Monte Carlo simulations. We find that the exponent m is approximately 0.5. In Fig. 3, the solid lines are fit to the data assuming a square root dependence of the bubble density on helium concentration. Thus the bubble density increases as the square root of the He/dpa ratio. While experimental evidence of this variation is difficult to find, such dependence has been suggested by rate theory calculations [30] for the case of cold helium implantation annealing. The square root dependence is also found for equilibrium bubbles containing an ideal gas [31].

We find that the bubble density increases with damage (expressed as dpa) as damage is accumulated till 1 dpa. At higher dpa ratios more vacancies are produced that may serve as nucleation sites for embryonic bubbles by trapping helium. Thus the bubble density scales directly with increasing damage. That bubble density increases with accumulating dpa is observed in experiments [7,8,32]. These experiments suggest much smaller values of bubble density than those calculated in the present simulations. Embryonic bubbles are submicroscopic and difficult to estimate from experimental observations; while the kMC simulations have a large fraction of nanometer size bubbles; making comparison with experiment difficult.

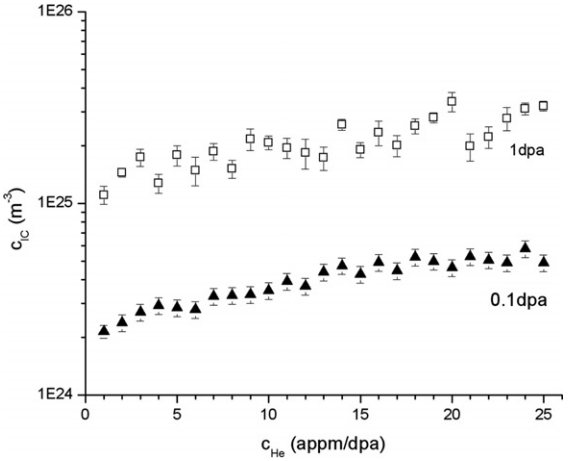

Fig. 4. A plot of the concentration of interstitial clusters (c_{IC}) as a function of helium concentration (expressed in terms of appm/dpa) for two damage levels, 0.1 dpa (filled triangles) and 1 dpa (open squares). The simulation temperature is 543 K (0.3 T_m, the melting temperature for iron).

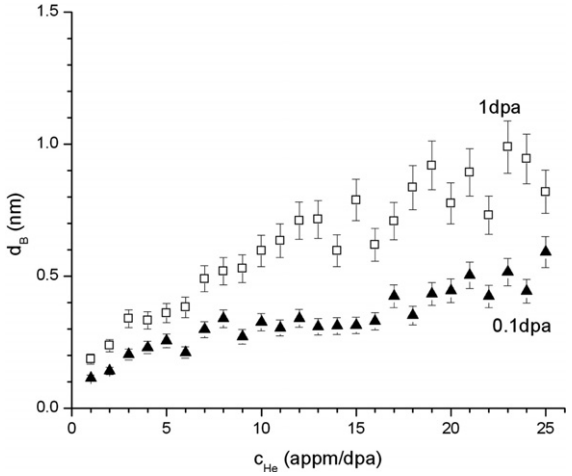

Fig. 5. A plot of the concentration of average bubble size (d_B expressed in nm) as a function of He concentration (expressed in terms of appm/dpa) for two damage levels, 0.1 dpa (filled triangles) and 1 dpa (open squares). The simulation temperature is 543 K (0.3 T_m, the melting temperature for iron).

Fig. 4 is a plot of the concentration of interstitial clusters as a function of the helium concentration expressed as an appm He/dpa ratio. Two different damage levels are considered 0.1 and 1 dpa. The simulation temperature is 0.3 T_m. There is a slight increase in interstitial cluster density with increasing helium concentration. This increase does not seem to be in agreement with experimental observations [7,8] that suggest that the interstitial loop size is independent of helium concentration. The assumption in the kMC simulation that interstitial clusters greater than 5 are immobile may contribute to the dependence of the interstitial cluster density on helium concentration. Such an assumption leads to interstitial clusters of larger size remaining in the simulation rather than being annealed to the boundaries. Post irradiation annealing simulations of this data may lead to a decrease in the interstitial cluster size as well. At present such annealing simulations have not been performed.

Fig. 5 is a plot of the bubble size as a function of the helium concentration expressed as an appm He/dpa ratio. As before two different damage levels are considered, namely 0.1 and 1 dpa and the simulation temperature is 0.3 T_m. Bubble size increases with increasing helium content and with increasing damage (dpa). The existing helium–vacancy bubbles act as sinks for the increasing helium and vacancies and trap these to increase the bubble size. As more vacancies are created, they are trapped at embryonic helium–vacancy bubbles thus increasing the bubble size with increasing dpa.

4. Discussion

Irradiation damage affects metal microstructure in several ways. It directly creates atomic defects and defect clusters and gradually modifies the pre-existing dislocation network. It introduces new impurities by nuclear transmutation. The transmutation gas so introduced affects the stability of vacancy clusters forming gas bubbles that serve as sinks for newly created vacancies and gas. The migration mechanisms of helium and hydrogen atoms in metals undergoing radiation damage are rather complex. In the present paper, we have analyzed various gas migration mechanisms and diffusion mediated reactions that lead to the nucleation of embryonic gas bubbles with a kinetic Monte Carlo (kMC) model and simulation. The bubble density scales linearly with increasing damage and increases as the square root of the He/dpa ratio at higher He/dpa ratios. The power law dependence of the bubble density agrees qualitatively with predictions of rate theory models that predict a fractional power law dependence of bubble density [30].

We have studied the interplay between various transmutation gas migration mechanisms in idealized situations. These models provide much insight

into the nature of embryonic gas bubble formation and growth. In these simulations, input information on defect interactions, mobilities, cluster stabilities, etc., is obtained from results of MD simulations and experimental measurements. Thus the accuracy of the kMC simulation is as good as the input parameters that are passed to it.

There is also debate as to the lowest-energy configuration of extrinsic gas atoms. Most classical interatomic potentials [19,20,22] yield the octahedral site as the lowest-energy configuration; recent first principles calculations [23,33] have suggested that the tetrahedral site may be lower in energy. Gas atoms in the present simulations diffuse on the octahedral sublattice. The simulation procedure may be changed to include diffusion on the tetrahedral sublattice; however, we do not believe that this will qualitatively change the results in term of the kinetics of defect migration or clustering behavior.

Similarly, in the kMC simulation, we have assumed that the lowest-energy migration path of the SIA corresponds to a nearest-neighbor translation–rotation jump in the $\langle 1\,1\,1\rangle$ direction as calculated by first principles calculations [23,28]. These calculations also suggest other paths of self interstitial atom migration; these at present are not included in the kMC simulations; however these can be easily incorporated. We do not expect these to affect the variation of the bubble density or cluster density with control parameters as the barrier for these mechanisms are higher than the barrier for the nearest neighbor translation rotation jump that is included in the present simulation.

The only work along such lines for the Fe–He system has been performed by the following: Morishita et al., Wirth and co-workers [19,20] and Wirth and Bringa [22]. In one paper, Morishita et al. [20] performed molecular dynamics (MD) calculations to evaluate the thermal stability of helium–vacancy clusters in Fe using the Ackland Finnis–Sinclair potential, the Wilson–Johnson potential and the Ziegler–Biersack–Littmark–Beck potential for describing the interactions of Fe–Fe, Fe–He and He–He, respectively. In another paper, Morishita et al. [19] have looked at dissolution of helium–vacancy clusters as a function of temperature increase using the empirical potentials for the Fe–He system. Using the same potential system to describe Fe–He and a kinetic lattice Monte Carlo model, Wirth and Bringa [22] have simulated the motion of one single 2He–3Vac cluster at 1000 K. In that paper, two interstitial helium atoms were placed in close proximity to a tri-vacancy cluster. The two helium atoms were found to cluster with the vacancy cluster within ~100 ps. In this paper, we have examined the nucleation and growth of helium–vacancy clusters that serve as embryonic bubbles during microstructural evolution over much larger time scales under continuous radiation damage conditions.

The bubble size and density dependence may have implications for the consideration of irradiation hardening. As the damage levels in structural materials increase, these materials show an increase in the yield stress. The increase in the yield stress is related to the interaction of dislocations with obstacles produced by the radiation damage. Often the increasing yield stress is described by the dispersed barrier hardening model [32,34],

$$\Delta\sigma = M\alpha\mu b\sqrt{Nd}, \tag{6}$$

where, $\Delta\sigma$ is the increase in yield stress, α is the strength of the dislocation obstacle interaction (between 0 and 1), M is the Taylor factor for bcc metals (~3.05), μ the shear modulus and b the dislocation burgers vector. The quantities N and d are the number density and diameter of the obstacles. If bubbles are assumed to interact with dislocation by such a relationship, the number density and the bubble size can be calculated by kMC calculations as shown in this paper and employed as parameters in continuum level plasticity calculations of irradiation hardening. Such a connection follows the chart shown in Fig. 1 where the atomistic information (defect migration energetics) is connected to macroscopic properties (change in yield stress) of the irradiated material.

5. Summary

We have employed kinetic Monte Carlo simulations to investigate the time evolution of the point defect configuration leading to defect clustering and bubble formation. The concentration and composition of embryonic defect clusters as a function of time and operating temperatures is determined. We have employed the kMC model to simulate the effect of damage and helium/dpa ratios on the formation of bubbles and bubble density. Simulations are performed for values of the He concentrations varying from 1 to 25 He/dpa. The bubble density scales linearly with increasing damage and increases as the square root of the He/dpa ratio at higher He/dpa ratios. Interstitial cluster density shows a slight dependence on the helium

concentration while bubble size increases with increasing helium content. Kinetic Monte Carlo simulations can be used to bridge the gap between atomistic molecular dynamics calculations and continuum level representations of irradiation hardening and mechanical property changes.

References

[1] M.S. Wechsler, K.L. Murty, Metall. Trans. A 20A (12) (1989) 2637.
[2] F. Garner et al., J. Nucl. Mater. 296 (2001) 66.
[3] S. Maloy et al., J. Nucl. Mater. 318 (2003) 283.
[4] S.A. Maloy et al., 3rd Workshop on Utilisation and Reliability of High Power Proton Accelerators, OECD, (2003), 105–124.
[5] B.M. Oliver et al., American Society for Testing and Materials Special Technical Publication, 20th International Symposium on Effects of Radiation on Materials 1045 (2001) 612–630.
[6] B.M. Oliver, M.R. James, F.A. Garner, S.A. Maloy, J. Nucl. Mater. 307 (2002) 1471.
[7] B.H. Sencer et al., American Society for Testing and Materials Special Technical Publication, 20th International Symposium on Effects of Radiation on Materials 1045 (2001) 588.
[8] B.H. Sencer, F.A. Garner, D.S. Gelles, G.M. Bond, S.A. Maloy, J. Nucl. Mater. 307 (2002) 266.
[9] H. Trinkaus, B. Singh, M. Victoria, J. Nucl. Mater. 237 (1996) 1089.
[10] H. Trinkaus, B.N. Singh, J. Nucl. Mater. 323 (2–3) (2003) 229.
[11] C.S. Becquart, C. Domain, L. Malerba, A. Hou, Nucl. Instr. and Meth. Phys. B 228 (2005) 181.
[12] C. Domain, C.S. Becquart, L. Malerba, J. Nucl. Mater. 335 (1–3) (2004) 121.
[13] F. Gao, D.J. Bacon, A.V. Barashev, H.L. Heinisch, Materials Research Society Symposium – Symposium on Microstructural Processes in Irradiated Materials 540 (1999) 703.
[14] H.L. Heinisch, B.N. Singh, Philos. Mag. 83 (31–34) (2003) 3661.
[15] H.L. Heinisch, B.N. Singh, S.I. Golubov, J. Nucl. Mater. 276 (2000) 59.
[16] A.V. Barashev, D.J. Bacon, S.I. Golubov, Materials Research Society Symposium – Symposium on Microstructural Processes in Irradiated Materials 540 (1999) 709.
[17] A.V. Barashev, D.J. Bacon, S.I. Golubov, J. Nucl. Mater. 276 (1) (2000) 243.
[18] M.J. Caturla, N. Soneda, T.D. De La Rubia, M. Fluss, J. Nucl. Mater. 351 (1–3) (2006) 78.
[19] K. Morishita, R. Sugano, B.D. Wirth, J. Nucl. Mater. 323 (2–3) (2003) 243.
[20] K. Morishita, R. Sugano, B.D. Wirth, T.D. De La Rubia, Nucl. Instr. and Meth. Phys. B 202 (2003) 76.
[21] E.M. Bringa, B.D. Wirth, M.J. Caturla, J. Stolken, D. Kalantar, Nucl. Instrum. and Meth. B 202 (suppl.) (2003) 56.
[22] B.D. Wirth, E.M. Bringa, Phys. Scr. T108 (2004) 80.
[23] C.-C. Fu, F. Willaime, Phys. Rev. B: Conds. Mat. Mater. Phys. 72 (6) (2005) 64117.
[24] J.H. Evans, J. Nucl. Mater. 334 (1) (2004) 40.
[25] G.A. Cottrell, Fus. Eng. Des. 66–68 (2003) 253.
[26] A.B. Bortz, M.H. Kalos, J.L. Lebowitz, J. Comput. Phys. 17 (1) (1975) 10.
[27] K.A. Fichthorn, W.H. Weinberg, J. Chem. Phys. 95 (2) (1991) 1090.
[28] C.-C. Fu, F. Willaime, P. Ordejon, Phys. Rev. Lett. 92 (17) (2004) 175503.
[29] ASTM E693, Annual Book of ASTM Standards, 12 February 1994.
[30] B.N. Singh, H. Trinkaus, J. Nucl. Mater. 186 (2) (1992) 153.
[31] A.J. Marksworth, Metall. Trans. 4 (11) (1973) 2651.
[32] S.J. Zinkle, N. Hashimoto, Y. Matsukawa, R.E. Stoller, Y.N. Osetsky, Materials Research Society Symposium – Radiation Effects and Ion-Beam Processing of Materials 792 (2003) 3.
[33] T. Seletskaia, Y. Osetsky, R.E. Stoller, G.M. Stocks, Phys. Rev. Lett. 94 (4) (2005) 046403.
[34] S.J. Zinkle, Y. Matsukawa, J. Nucl. Mater. 329–333 (1–3 Part A) (2004) 88.